Journal of Korean Association of Crystal Growth
Vol. 9, No. 1 (1999) 94-100

Effects of stabilizing temperature gradients on thermal convection in rectangular enclosures during physical vapor transport

Geug-Tae Kim, Jang-Woo Choi, Min-Ok Lee, Moo Hyun Kwon* and Soon Kil Kwon**

Department of Chemical Engineering, Hannam University, Taejon 306-791, Korea
**Department of Chemical Engineering, KAIST, Taejon 305-701, Korea*
***Agency for Defense Development, Taejon 305-600, Korea*
(Received December 1, 1998)

승화법에 의한 단결정성장공정에서 이중온도구배가 대류현상에 미치는 영향

김극태, 최장우, 이민옥, 권무현*, 권순길**

한남대학교 화학공학과, 대전, 306-791
*한국과학기술원 화학공학과, 대전, 305-701
**국방과학연구소, 대전, 305-600
(1998년 12월 1일 접수)

Abstract Mercurous chloride (Hg_2Cl_2) crystals hold promise for many acousto-optic and opto-electronic applications, which are prepared in closed ampoules by the physical vapor transport (PVT) growth methods. The thermal boundary conditions established by imposing different temperature on sidewalls of the enclosure cause simultaneous horizontal and vertical convective flow in the PVT processes of Hg_2Cl_2. It is found that for the ratios of horizontal to vertical thermal Rayleigh numbers $Ra_H/Ra \geq 1.5$, the convective flow structure changes from multicellular to unicellular for the base parametric state of $Ra = 2.79\times10^4$, $Pr = 0.91$, $Le = 1.01$, $Pe = 4.60$, $Ar = 0.2$ and $C_v = 1.01$. For the ΔT^*_H greater than 0.3, the $|U|_{max}$ is increased with increasing ΔT^*_H and decreasing the aspect ratio. For the aspect ratios ranging from 0.1 to 1.0, there is a direct and linear relationship between $|U|_{max}$ and $\sqrt{\Delta T^*_H}$. A decrease in the aspect ratio destabilizes the convective flow and results in an increase of the magnitude of convection in the crystal growth reactor. The vertical gradient tends to destabilize the convective flow which leads to oscillations, whereas the horizontal gradient stabilizes the convection.

요 약 음향광 소재와 광전자 재료용으로 적합한 염화제일수은은 밀폐된 용기에서 승화법에 의한 결정성장으로 제조된다. 온도경계조건으로 밀폐된 용기의 측면에 각각 다른 온도로 부하하였을 때에는 수직적과 수평적 대류현상이 동시에 일어난다. 수직적 레이 무차원수에 대한 수평적 레이 무차원수의 비율이 1.5 보다 클 때, 대류유동구조는 $Ra = 2.79\times10^4$, $Pr = 0.91$, $Le = 1.01$, $Pe = 4.60$, $Ar = 0.2$ and $C_v = 1.01$에서 한 개의 셀에서 여러 개의 셀로 변한다. $\Delta T^*_H \geq 0.3$에 대하여, ΔT^*_H의 증가함과 엑스펙트 비율의 감소함에 따라 $|U|_{max}$이 증가한다. 0.1에서 1까지의 엑스펙트 비율의 범위에서는 $|U|_{max}$가 $\sqrt{\Delta T^*_H}$와 직접적이며 선형적인 관계에 있다. 엑스페트 비율이 감소함에 따라 대류의 흐름은 불안정하게 되며, 그 결과 대류의 크기는 증가한다. 수직적 온도구배는 대류의 흐름을 불안정하게 하여 진동하게 하며, 그 반면에 수평적 구배는 흐름을 안정화시킨다.

1. Introduction

Interest in growing Hg_2Cl_2 single crystal stems from their exceptional optical properties and very broad transmission range from 0.36 to 20 μm for applications in acousto-optic and opto-electronic devices such as Bragg cells, X-ray detectors operating at ambient temperature [1]. Because of decomposition of Hg_2Cl_2 into Hg and $HgCl_2$ at a melting point of 525℃ [2, 3], these crystals are usually grown by the physical vapor transport (PVT) in closed silica glass ampoules. The vapor pressure of Hg_2Cl_2 at operating temperature ranges from 290℃ to 320℃, far below the melting point, varies from 50 torr to

150 torr [4] so that the PVT method is suitable for its growth. The mechanism of the PVT process is simple : sublimation-condensation in closed silica glass ampoules in temperature gradient imposed between the source material and the growing crystal. In the PVT system of Hg_2Cl_2, the molecular species Hg_2Cl_2 sublimes as the vapor phase from the crystalline source material (Hg_2Cl_2), and is subsequently transported and re-incorporated into the single crystalline phase (Hg_2Cl_2) [5]. Thermal convection is attributable to interaction of a gravitational acceleration with the density gradients resulting from the temperature gradients for the PVT processes on earth. The understanding and control of PVT processings have been hampered by such an unavoidable convection under ground-based experimental conditions.

The laser Doppler velocimetry (LDV) measurements of Hg_2Cl_2 vapor were performed in the PVT system; the asymmetrical wall temperature profiles are inevitably generated by the use of a modified two-zone furnace [6]. The velocity profile measurements indicate a presence of asymmetric convective cell for a fixed axial location. In the absence of the measurement of the entire flow field, however, the possibility of vertically ordered asymmetric multicells exists. One would ask a question whether the asymmetric temperature gradients cause a single cell or a vertically ordered multicellular structure in the flow field. Motivated by this uncertainty we investigate the trends in the convective flow behavior, the effect of asymmetrically imposed temperature profiles on the flow field structure, and the likelihood of a presence of multicells in the flow field. Moreover, asymmetrical temperature profiles affect the convective flow structures within crystal growth ampoules which are directly related crystal quality. The effect of thermal boundary conditions on natural convection of confined fluids is of considerable importance in application to PVT crystal growth.

In this paper we consider a two-dimensional model based on rectangular geometry for the prediction of nonaxisymmetrical flow fields; the experiments show that the convective flow structures are asymmetric [6]. This paper will present the effect of stabilizing temperature gradients on thermal convection for various aspect ratios (width-to-transport length) from 0.1 to 1.0. Note this paper is an extension of ref. [7] which dealt with an aspect ratio of 0.2 only.

2. Mathematical and physical formulations

Consider a rectangular enclosure of width H and transport length L, shown in Fig. 1. The source is maintained at a temperature T_s, while the growing crystal is at a temperature T_c, with $T_s > T_c$. PVT of the transported component A occurs inevitably, due to presence of impurities, with the presence of an inert component B; to address thermal convection we assume that the impurity B has the same molecular weight as the component A, which indicates the self-diffusion limit in the PVT processes. We also assume the impurity B has a slight excess pressure and both the sublimation and condensation of a mixture of A (Hg_2Cl_2) and B (impurity) occur congruently. The interfaces are assumed to be flat for simplicity. The finite normal velocities at the interfaces can be expressed by Stefan flow deduced from the one-dimensional diffusion-limited model [8-10], which provide the coupling between the fluid dynamics and species calculations. On the other hand, the tangential component of the mass average velocity of the vapor at the interfaces vanishes. Thermodynamic equilibria are assumed at the interfaces so that the mass fractions at the interfaces are kept constant at $\omega_{A,s}$ and $\omega_{A,c}$. On the vertical

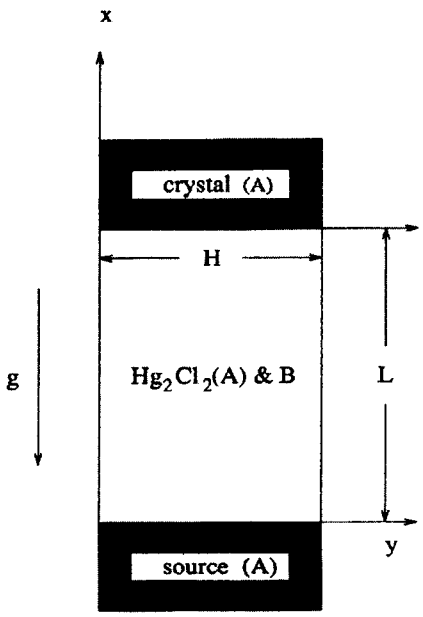

Fig. 1. Schematic description of the physical vapor transport crystal growth reactor in a rectangular system.

non-reacting walls an appropriate velocity boundary condition is no-slip, the normal concentration gradient is zero, and temperature is imposed as a linear temperature gradient and an asymmetric horizontal temperature gradient. The asymmetry is attributable to temperature differences between two opposite walls.

The transport of fluid within a rectangular PVT crystal growth reactor is governed by a system of elliptic, coupled conservation equations for mass (continuity), momentum, energy and species (diffusion) with their appropriate boundary conditions. Let v_x, v_y denote the velocity components along the x- and y-coordinates in the x, y rectangular coordinate, and let T, ω_A, p denote the temperature, mass fraction of species A (Hg_2Cl_2) and pressure, respectively.

The dimensionless governing equations are given by:

$$\nabla^* \bullet \vec{V}^* = 0, \tag{1}$$

$$\vec{V}^* \bullet \nabla^* \vec{V}^* = -\nabla^* p^* + Pr \nabla^{*2} \vec{V}^* - Ra \cdot Pr \cdot T^* \cdot e_g, \tag{2}$$

$$\vec{V}^* \bullet \nabla^* T^* = \nabla^{*2} T^* \tag{3}$$

$$\vec{V}^* \bullet \nabla^* \omega_A^* = \frac{1}{Le} \nabla^{*2} \omega_A^* \tag{4}$$

These nonlinear, coupled sets of equations are numerically integrated with the following boundary conditions:

On the source ($x^* = 0$, $0<y^*<1$):

$$u(0, y^*) = -\frac{1}{Le} \frac{\Delta\omega}{(1-\omega_{A,s})} \frac{\partial \omega_A^*(0, y^*)}{\partial x^*}, \tag{5}$$

$$v(0, y^*) = 0,$$

$$T^*(0, y^*) = 1,$$

$$\omega_A^*(0, y^*) = 1,$$

On the walls ($0<x^*<L/H$, $y^* = 0$ and 1):

$$u(x^*, 0) = u(x^*, 1) = v(x^*, 0) = v(x^*, 1) = 0 \tag{6}$$

$$\frac{\partial \omega_A^*(x^*, 0)}{\partial y^*} = \frac{\partial \omega_A^*(x^*, 1)}{\partial y^*} = 0,$$

$$T^*(x^*, 0) = -Ar \cdot x^* + 1 \text{ and}$$

$$T^*(x^*, 1) = -Ar \cdot x^* + 1 + \Delta T_H^*$$

On the crystal ($0<x^*<L/H$, $y^* = 0$ and 1):

$$u(L/H, y^*) = -\frac{1}{Le} \frac{\Delta\omega}{(1-\omega_{A,c})} \frac{\partial \omega_A^*(L/H, y^*)}{\partial x^*} \tag{7}$$

$$v(L/H, y^*) = 0,$$

$$T^*(L/H, y^*) = 0,$$

$$\omega_A^*(L/H, y^*) = 0,$$

where Ra, Pr , Le , Pe, Ar are defined in the ref. [7].

3. Numerical methods

The discretization equations for a set of conservation equations are solved using a finite-volume-formulated SIMPLER (Semi-Implicit Method Pressure-Linked Equations Revised) algorithm proposed by Patankar [11], with a power law scheme. A line-by-line solution method, which utilizes a tridiagonal matrix algorithm for the solution along each line of unknowns, is used to solve the discretization equations for the individual variables. Also, a staggered grid is used in order to avoid a wavy velocity field.

The 23×43 grids are found to be able to reveal the essential features of the transport process. The iteration procedure is continued until the following convergence criterion is satisfied:

$$\left| \frac{\phi_{j+1} - \phi_j}{\phi_j} \right| < 10^{-5} \qquad \text{for all } \phi,$$

where ϕ represents any dependent variable being computed, e.g., u, w, temperature and species, and j refers to the value of ϕ at the jth iteration level.

4. Results and discussion

Two-dimensional rectangular numerical studies are investigated for $p_B = 133$ Pascal, $T_s = 320$℃, $\Delta T = 30$ K, $Ra = 2.79\times10^4$, $Pr = 0.91$, $Le = 1.01$, $Pe = 4.60$, $C_v = 1.01$, $0.1\le Ar\le1.0$ and $0\le T_H\le60$ K. Variations in ΔT_H are obtained by raising the temperature of one side of the wall at $y^* = 1$ relative to that at $y^* = 0$, while ΔT is held constant.

Figure 2 shows regimes for convective flow fields and transition from steady to transient convection for various aspect ratios ($0.1\le Ar\le1.0$) and horizontal Rayleigh numbers ($0\le Ra_H\le5.58\times10^4$). For ΔT^*_H greater than 0.57, the convective flows exhibit the steady state characteristics for $0.1\le Ar\le1.0$. The convective flows transit from the oscillatory to the steady state convective mode with increasing the aspect ratio as well as the Ra_H.

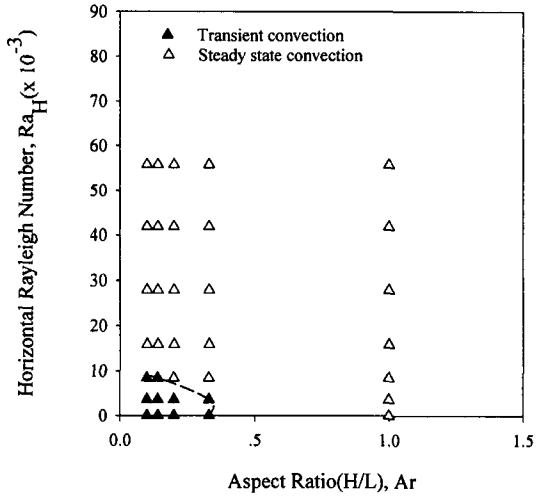

Fig. 2. Convective modes for various aspect ratios ($0.1 \leq Ar \leq 1.0$) and horizontal Rayleigh numbers ($0 \leq Ra_H \leq 5.58 \times 10^4$).

Note $Ra_H = 0$ means that asymmetrical temperature gradients are absent. The case of $Ra_H = 0$ and $Ar = 1.0$ shows the steady state mode, indicating the greater the aspect ratio, the stabler the convective flow behaviors. The definition of Ra_H is found in the ref. [7]. For $\Delta T^*_H \leq 0.3$ for $Ar = 0.1$ and 0.14, 0.13 for $Ar = 0.2$ and 0.33, the convective flows seem to be oscillatory so that numerical convergences are very difficult to achieve. The convective flow fields are likely to be oscillatory, which is evident from the difference in $|U|_{max}$.

$|U|_{max}$ is used as a representation for checking oscillation of the flow field, the strength of convection for each case [12]. The effects of asymmetric horizontal temperature profiles, ΔT_H, on the nature of the flow field are typically illustrated by plots of velocity vectors, streamline and temperature contours, and concentration profiles in Figs. 3 and 4. The flow fields for $\Delta T^*_H = 0.13$ and $Ar = 0.2$ shows that three dominant cells and a secondary cell near the crystal are predicted (Fig. 3), which indicates convective oscillation. Therefore, in the vertical cavity under considerations the convective flow seems to be inherently oscillatory for the horizontal temperature gradients ΔT^*_H smaller than or equal to 0.13 ($Ra_H \geq 3.6 \times 10^3$) with the aspect ratios Ar ranging from 0.1 to 0.33, shown in Fig. 2. In the velocity field shown in Fig. 4 for $\Delta T^*_H = 1.0$ and $Ar = 0.2$, it is apparent that secondary cells occur near the crystal and source regions; the core of the

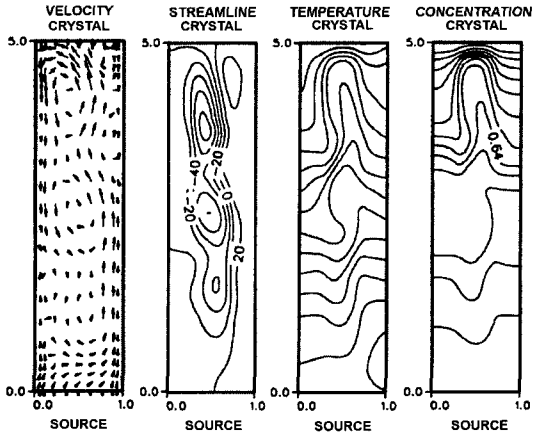

Fig. 3. Velocity ($|U|_{max} = 3.25$ cm/s), streamline ($\psi_{max} = 48.82$, $\psi_{min} = -90.53$, $\Delta\psi = 20.0$), temperature ($\Delta T^* = 0.08$), and mass concentration fields ($\Delta\varpi^*_A = 0.08$), $\Delta T^*_H = 0.13$, $Ar = 0.2$.

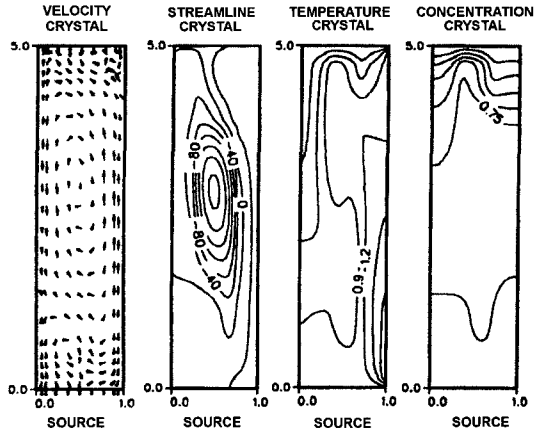

Fig. 4. Velocity ($|U|_{max} = 8.79$ cm/s), streamline ($\psi_{max} = 71.40$, $\psi_{min} = -251.50$, ($\Delta\psi = 40.0$), and mass concentration fields ($\Delta\varpi^*_A = 0.15$), $\Delta T^* = 0.30$, $\Delta T^*_H = 1.0$, $Ar = 0.2$.

enclosure has one large single cell. As ΔT^*_H is increased from 1.0 to 2.0 at $Ar = 0.2$, viz., the horizontal temperature difference ($\Delta T_H = 60$ K) becomes greater than the vertical one ($\Delta T_H = 30$ K), the two cells at the source and crystal regions are suppressed and a unicellular flow pattern arises (not shown). Also, the convective flow structure for $\Delta T_H = 45$ K remains basically the same as for $\Delta T_H = 60$ K, which is not shown here. Note that the temperature and concentration fields remain nonuniform near the crystal boundary. This implies that for $0.3 \leq \Delta T^*_H \leq 2.0$ ($8.37 \times 10^3 \leq Ra_H \leq 5.58 \times 10^4$, $Ar = 0.2$), the intensity of thermal convection due to the hori-

zontal temperature gradients (ΔT^*_H) is dominant over the intensity of thermal convection due to the vertical temperature gradients (ΔT^*). This is supported by the following observations (shown in Figs. 3 and 4): (1) the diameter of the roll of the main convection cell increases with increase in ΔT^*_H, (2) the main convection cell suppresses the small cells near the source and crystal, and (3) the motion of the dominant cell becomes more intense. Therefore, as ΔT^*_H increases, the vertical heat transfer mode (which gives rise to a vertical multicellular convection) is switched to the horizontal heat transfer mode responsible for a unicellular convection.

Figure 5 shows that for the five fixed parameters (Ra, Pr, Le, Pe and Cv), $|U|_{max}$ increases linearly with $\sqrt{\Delta T^*_H}$ for various aspect ratios, $0.1 \le Ar \le 1.0$. For the $\sqrt{\Delta T^*_H} > 0$, the $|U|_{max}$ increases with decreasing the aspect ratio, indicating the intensity of thermal convection is increased with an decrease in the aspect ratio. On the other hand, for $\Delta T^*_H = 0$, when the aspect ratio is decreased from 1 to 0.1 without changing the governing parameters of Ra, Pr, Le, Pe and C_v, $|U|_{max}$ changes from 3.0 to 1.5, which is consistent with the result of [12]. In other words, $|U|_{max}$ inversely increases with the aspect ratio when symmetrical temperature gradients are imposed on the sidewalls. Thus, this observation can be explained merely by the fact that in the absence of ΔT^*_H, the effect of side walls tends to retard the convection while for the higher $\sqrt{\Delta T^*_H}$ cases it accelerates the intensity of convection. The convection slowly increases with an increase in $\sqrt{\Delta T^*_H}$ and a decrease in the aspect ratio, which implies the horizontal temperature gradient was relatively significant for the lower aspect ratios than 1. Therefore, as the aspect ratio decreases, the effects of sidewalls tend to destabilize the convective flow and to increase the magnitude of convection. Figure 6 shows the dependence of $|U|_{max}$ on the aspect ratio for various ΔT^*_H, whereas Fig. 7 shows that for various aspect ratios, $0.1 \le Ar \le 1.0$, the $|U|_{max}$ increases with increasing ΔT^*_H except for $\Delta T^*_H = 0.0$ and 0.13. For low aspect ratios of $Ar = 0.1$ and

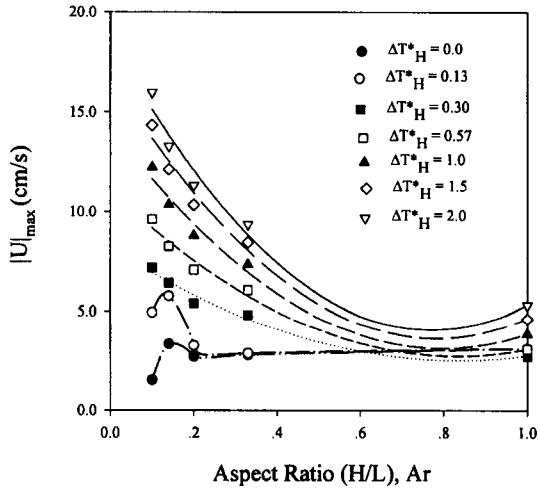

Fig. 6. Dependence of $|U|_{max}$ on the aspect ratio for various ΔT^*_H, $0.0 \le \Delta T^*_H \le 2.0$.

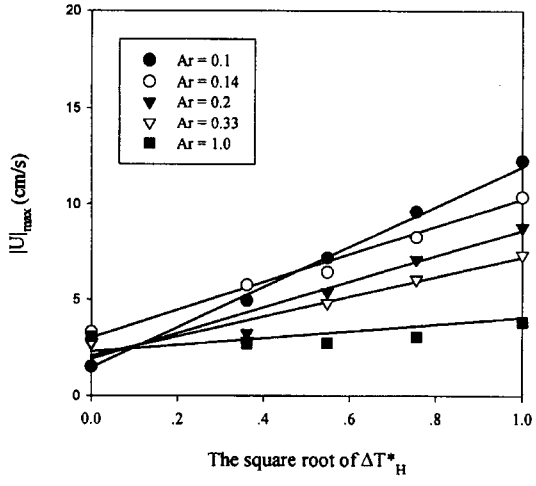

Fig. 5. Dependence of $|U|_{max}$ on the $\sqrt{\Delta T^*_H}$ for various aspect ratios, $0.1 \le Ar \le 1.0$.

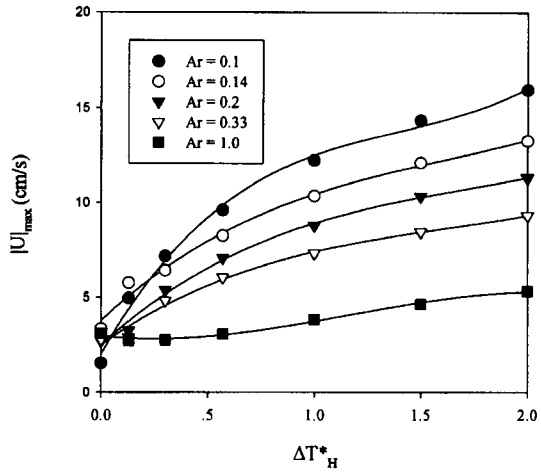

Fig. 7. Relationship between $|U|_{max}$ and ΔT^*_H for various aspect ratios, $0.1 \le Ar \le 1.0$.

0.14, the $|U|_{max}$ increases with the aspect ratio (Ar) until the Ar reaches the critical value. At the critical Ar, the $|U|_{max}$ abruptly decreases and then, slowly increases. Note the $|U|_{max}$ is directly proportional to the crystal growth rate. In Fig. 5 through 7, all symbols denote results obtained numerically and all lines are obtained through statistical regressions for the corresponding symbols.

In regards to fluid flow driven by a horizontal temperature gradient in rectangular enclosures (conventional thermal convection), as the ratio of vertical to horizontal Rayleigh numbers increases, the flow velocity is decreased, shown in Fig. 5 through 7. This tendency is with the experimental results of Ostrach and Raghavan [13] for silicone oils rectangular enclosures. The vertical gradient tends to destabilize the flow which leads to oscillations. Aside from the effects of mass fluxes at the solid-vapor interfaces, for conventional thermal convection problems with parametric ranges similar to our study, an increase in the ratio of the vertical to horizontal Rayleigh number tends to destabilize the flow. On the other hand, for a given vertical Rayleigh number, a decrease in the ratio of vertical to horizontal Rayleigh number stabilizes the flow.

5. Conclusions

The unicellular convective flow structure occurs in a system with $Ra = 2.79 \times 10^4$, $Pr = 0.91$, $Le = 1.01$, $Pe = 4.60$, $Ar = 0.2$, $C_v = 1.01$ for the ratios of $Ra_H/Ra \geq 1.5$. In the laser Doppler velocimetry experiments with asymmetric horizontal temperature gradients [6] a unicellular flow structure is not likely to occur because $\Delta T^*_H \leq 1.0$ for the experiments. The horizontal asymmetric temperature gradients increase the magnitude of convection due to the large temperature differences between opposite walls and has a stabilizing effect on the flow. At low ratios of Ra_H/Ra, the flow becomes unsteady and has the characteristics of vertical multicellular flow structure. This study implies that the convective flow field structure found in our experiments is likely to be multicellular. For a given vertical Rayleigh number, a decrease in the ratio of vertical to horizontal Rayleigh number stabilizes the flow. As the aspect ratio decreases, the effects of sidewalls tend to destabilize the convective flow and to increase the magnitude of convection in the crystal growth reactor.

Acknowledgement

The authors wish to acknowledge the financial support of the Korea Research Foundation made in the program year of 1997 (Non Directed Research Fund, Grant No. 1997-001-E00466).

Nomenclature

A	component A, Hg_2Cl_2
B	component B, impurity
D_{AB}	binary diffusivity of A and B
e_g	unit vector of gravity acceleration
g	standard gravitational acceleration constant, 980.665 cm/sec^2
H	width
L	transport length
p	pressure
p*	dimensionless pressure, $p/\rho_c U_c^2$
P_T	total pressure
T	temperature
T*	dimensionless temperature, $(T - T_c)/(T_s - T_c)$
ΔT	temperature difference between source and crystal, $T_s - T_c$
ΔT_H	wall-to-wall temperature difference, $T(x, H) - T(x, 0)$
ΔT^*_H	dimensionless wall-to-wall temperature difference, $T^*(x^*, 1) - T^*(x^*, 0)$
x	x-coordinate
x*	dimensionless x-coordinate, x/H
y	y-coordinate
y*	dimensionless x-coordinate, y/H
u	dimensionless x-coordinate velocity, v_x/U_c
U_c	characteristic velocity, κ/H
$\|U\|_{max}$	dimensional maximum magnitude of velocity vector
v	dimensionless y-component velocity, v_y/U_c
v_x	x-component velocity
v_y	y-component velocity

Dimensionless governing parameters

Ar	aspect ratio, H/ L
C_v	concentration parameter, $C_v = (1 - \varpi_A)/\Delta\varpi$
Le	Lewis number, κ/D_{AB}
Pe	Peclet number, $U_{adv} L/D_{AB}$
Pr	Prandtl number, ν/κ
Ra	Rayleigh number, $g \Delta T H^3/\kappa\nu$

Subscripts and superscripts

A	component A, Hg_2Cl_2
Adv	advection
B	component B
c	crystal
H	horizontal
s	source
T	total vapor pressure
□	dimensionless

Greek letters

β	thermal volume expansion
δ	increment of contour
κ	thermal diffusivity
μ	viscosity
∇^*	$\partial/\partial x^* + \partial/\partial y^*$
∇^{*2}	$\partial^2/\partial x^{*2} + \partial^2/\partial y^{*2}$
ν	kinematic viscosity
ϕ	variable (u, v, T^*, ϖ^*_A)
ψ	dimentionless streamline
ϖ_A	mass concentration of component A
$\Delta\varpi$	mass concentration difference between source and crystal, $\varpi_{A,s} - \varpi_{A,c}$
ϖ^*_A	dimensionless mass concentration, $(\varpi_A - \varpi_{A,c})/\Delta\varpi$
ρ	density of fluid with component A and B

References

[1] N.B. Singh, R.H. Hopkins, R. Mazelsky and J.J. Conroy, J. Crystal Growth 75 (1986) 173.
[2] S.J. Yosim and S.W. Mayer, J. Physical Chemistry 64 (1960) 909.
[3] N.B. Singh, R.H. Hopkins, R. Mazelsky and M. Gottlieb, J. Crystal Growth 83 (1987) 334.
[4] V.K. Newmann and E. Liehtenberg, Z. Phys. Chem. A 191 (1942) 224.
[5] N.B. Singh, M. Gottlieb, R.H. Hopkins, R. Mazelsky, W.M.B. Duval and M.E. Glicksman, Prog. Crystal Growth and Charact. 27 (1993) 201.
[6] G.T. Kim, J.T. Lin, O.C. Jones, W.M.B. Duval, M.E. Glicksman and N.B. Singh, J. Crystal Growth 165 (1996) 429.
[7] G.T. Kim, W.M.B. Duval and M.E. Glicksman, Chem. Eng. Comm. 162 (1997) 45.
[8] W.M.B. Duval, Proc. ASME--WAM, Fluid mechanics phenomena in microgravity, AMD-Vol. 174, FED-Vol. 175 (New Orleans, Louisiana, 1993) 51.
[9] G.T. Kim, W.M.B. Duval, M.E. Glicksman and N.B. Singh, Modelling Simul. Mater. Sci. Eng. 3 (1995) 331.
[10] D.W. Greenwell, B.L. Markham and F. Rosenberger, J. Crystal Growth 51 (1981) 413.
[11] S.V. Patankar, Numerical Heat Transfer and Fluid Flow (Hemisphere Publishing Corp., Washington D.C., 1980).
[12] G.T. Kim, W.M.B. Duval and M.E. Glicksman, Modeling Simul. Mater. Sci. Eng. 5 (1997) 289.
[13] S. Ostrach and C. Raghavan, J. Heat Transfer 101 (1979) 238.